Bond versus charge disproportionation and nature of the holes in $s-p$ ABX_3 perovskites

Mohammad Reza Benam,* Kateryna Foyevtsova,† Arash Khazraie, Ilya Elfimov, and George A. Sawatzky
Department of Physics and Astronomy, University of British Columbia, Vancouver, British Columbia, Canada V6T 1Z1 and Stewart Blusson Quantum Matter Institute, University of British Columbia, Vancouver, British Columbia, Canada V6T 1Z4

(Received 20 April 2021; revised 15 October 2021; accepted 2 November 2021; published 22 November 2021)

We use density functional theory methods to study the electronic structures of a series of s-p cubic perovskites, ABX_3: the experimentally available $SrBiO_3$, $BaBiO_3$, $BaSbO_3$, $CsTlF_3$, and $CsTlCl_3$, as well as the hypothetical $MgPO_3$, $CaAsO_3$, $SrSbO_3$, and $RaMcO_3$. We use tight-binding modeling to calculate the interatomic hopping integrals $t_{sp\sigma}$ between the B s and X p atomic orbitals and charge-transfer energies Δ, which are the two most important parameters that determine the low-energy electron and hole states of these systems. Our calculations elucidate several trends in $t_{sp\sigma}$ and Δ as one moves across the periodic table, such as the relativistic energy lowering of the B s orbital in heavy B cations, leading to strongly negative Δ values. Our results are discussed in connection with the general phase diagram for s-p cubic perovskites proposed by Khazraie *et al.* [Phys. Rev. B **98**, 205104 (2018)], who find the parent superconductors $SrBiO_3$ and $BaBiO_3$ to be in the regime of negative Δ and large $t_{sp\sigma}$. Here, we explore this further and search for different materials with similar parameters, which could lead to the discovery of new superconductors. Also, some considerations are offered regarding a possible relation between the physical properties of a given s-p compound (such as its tendency to bond disproportionate and the maximal achievable superconducting transition temperature) and its electronic structure.

DOI: 10.1103/PhysRevB.104.195141

I. INTRODUCTION

Materials with the cubic perovskite structure ABX_3, where the anion X can be an oxygen or a halogen and the possible cations A and B include a broad variety of elements or even molecules, have attracted considerable attention due to their rich physics. Indeed, among their intriguing properties are metal-insulator transitions [1,2], high transition temperature T_c superconductivity [3–5], ferroelectricity, ferromagnetism, applicability to photovoltaics [6], colossal magnetoresistance [7], magnetoelectricity [8], and a topological insulating state [9–11]. The crystal structure of the ABX_3 cubic perovskites consists of a three-dimensional network of corner-sharing BX_6 octahedra intercalated with A cations at the 12-fold anion-coordinated sites. One of the well-known and widely studied ABX_3 compounds is $ABiO_3$, with A = Ba or Sr. Upon hole doping, achieved via chemical substitutions, these systems become superconducting with a surprisingly high maximal T_c of 30 K [4,5,12,13]. As stoichiometry is approached in the pure parent compound, however, the superconductivity gives way to an insulating state featuring a so-called breathing structural distortion, where the BiO_6 octahedra disproportionate into small and large ones in a rocksaltlike pattern [14–17].

Although in the early years following the discovery of $ABiO_3$ their breathing distortion was viewed as a result of charge disproportionation of the nominally tetravalent Bi^{4+} ions into Bi^{3+} and Bi^{5+}[18–20], recent theoretical [21–26] and experimental [27–32] studies have seriously challenged this idea. In a more realistic microscopic picture, developed by some of us in Refs. [23,24,26], one starts by recognizing the negative charge-transfer nature of the $ABiO_3$ electronic states, i.e., that the O $2p$ states are, in fact, higher in energy than the semicore Bi $6s$ states (by the amount Δ), as depicted in the top panel of Fig. 1(a). However, the most important parameter shaping the $ABiO_3$ electronic structure is the strong hybridization between the Bi $6s$ atomic orbital and the a_{1g} molecular orbital (MO) formed by the O $2p_\sigma$ orbitals of the oxygen octahedral cage [see Fig. 1(b)]. It produces a huge splitting between the bonding and antibonding bands that is much larger than the charge-transfer energy, with the latter band landing at the Fermi energy above the O nonbonding states, as depicted in the middle panel of Fig. 1(a). Since the character of the conductance antibonding band is predominantly that of the O a_{1g} MO, the average Bi oxidation state approaches 3+, leaving two self-doped ligand holes $\underline{L}$ per oxygen octahedron as $2Bi^{4+} \rightarrow 2Bi^{3+}\underline{L}^2$, in what Zunger and coworkers called a "self-regulating response" [25,33]. Upon the breathing distortion, resulting from the strong electron-breathing-phonon interaction, which increases the short-bond-length Bi $6s$-O $2p$ hopping integrals and therefore further stabilizes the bonding state, the ligand holes condense pairwise onto the small octahedra as $2Bi^{3+}\underline{L}^2 \rightarrow [Bi^{3+}]_{\text{large}} + [Bi^{3+}\underline{L}^2]_{\text{small}}$, resulting in nearly the same valence states for the two inequivalent Bi ions [23], a situation that should be called bond, rather than charge, disproportionation. As shown in the bottom panel of Fig. 1(a), this process is associated with opening of a charge gap at the center of the antibonding band of the cubic structure.

With this picture of the $ABiO_3$ electronic structure in mind, a further step was taken in Ref. [26], and a general phase diagram was proposed to describe a crossover from a bond- to a charge-disproportionated regime in s-p cubic perovskites

*Present address: Department of Physics, Payame Noor University, P.O. Box 19395-3697, Tehran, Iran.
†foyevtsova@phas.ubc.ca

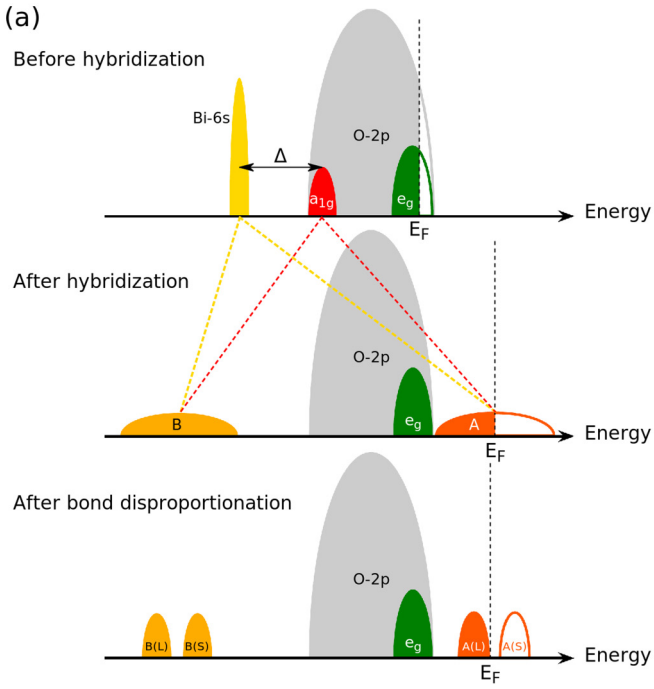

(b)

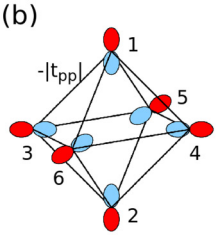

O site	a_{1g}	t_{1u}	t_{1u}	t_{1u}	e_g	e_g
1	1/√6	1/√2	0	0	1/√3	0
2	1/√6	-1/√2	0	0	1/√3	0
3	1/√6	0	1/√2	0	-1/√12	1/2
4	1/√6	0	-1/√2	0	-1/√12	1/2
5	1/√6	0	0	1/√2	-1/√12	-1/2
6	1/√6	0	0	-1/√2	-1/√12	-1/2
Energy	$-4\|t_{pp}\|$	0	0	0	$2\|t_{pp}\|$	$2\|t_{pp}\|$

FIG. 1. (a) Schematic diagram of the Bi 6*s* and O 2*p* energy levels in $ABiO_3$ before (top panel) and after (middle panel) hybridization. A and B denote antibonding and bonding bands, respectively. The bottom panel demonstrates the effect of Bi-O bond disproportionation, whereby the bonding and the antibonding bands are each split into two subbands associated with large and small BiO_6 octahedra, denoted as B(L), B(S), A(L), and A(S), respectively, and a charge gap is opened as a result. (b) The six O $2p_\sigma$ orbitals of an O_6 octahedron and their molecular orbital combinations, a_{1g}, t_{1u}, and e_g, with their corresponding energies given in units of the nearest-neighbor hopping integral $-|t_{pp}| = \frac{1}{2}[(pp\sigma) + (pp\pi)]$, where $(pp\sigma)$ and $(pp\pi)$ are the Slater-Koster parameters.

similar to $ABiO_3$. It was shown that there are two main electronic parameters that determine the regime a given system will end up in: the charge-transfer energy Δ and the hybridization between the *B* cation *s* orbital and the oxygen a_{1g} MO characterized by the hopping integral $T_{sp\sigma} = \sqrt{6}t_{sp\sigma}$, where $t_{sp\sigma}$ is the interatomic hopping integral between the *B* cation *s* orbital and the oxygen p_σ orbital. However, even though a number of *s*-*p* cubic perovskites other than $ABiO_3$ are known, such as the recently synthesized $CsTlCl_3$ and $CsTlF_3$ [34], and some of them even superconduct ($BaPb_{1-x}Sb_xO_3$ [35,36], $Ba_{1-x}K_xSbO_3$ [37]), no real examples were discussed in Ref. [26] in relation to the proposed phase diagram. In order to fill this gap, in the present paper we use *ab initio* theoretical methods to study the electronic structures of the above-mentioned existing *s*-*p* cubic perovskites and also of a systematic series of hypothetical ABO_3 systems, with *A* and *B* cations being the group IIa and group Va elements, respectively. We hope that this study, conducted in light of the notion of charge versus bond disproportionation, will add to our understanding of superconductivity in the *s*-*p* cubic perovskites and also guide the discovery of new superconductors.

TABLE I. GGA equilibrium lattice constants *a*, *B s*-*X p* hopping integrals $t_{sp\sigma}$, and charge-transfer energies Δ of the studied ABX_3 cubic perovskites.

	Synthesized?	*a* (Å)	$t_{sp\sigma}$ (eV)	Δ (eV)
$MgPO_3$	No	3.667	2.65	1.83
$CaAsO_3$	No	3.919	2.30	−1.44
$SrSbO_3$	No	4.233	2.08	−1.08
$BaSbO_3$	Yes [36,37]	4.280	2.01	−1.53
$SrBiO_3$	Yes [13]	4.372	1.88	−3.68
$BaBiO_3$	Yes [4]	4.417	1.81	−3.96
$RaMcO_3$	No	4.676	1.46	−8.86
$CsTlF_3$	Yes [34]	4.799	1.24	0.65
$CsTlCl_3$	Yes [34]	5.604	1.16	−0.88

II. METHOD

Our electronic structure calculations are performed within density functional theory (DFT) [38] using the full-potential linearized augmented plane-wave method and the scalar-relativistic approximation as implemented in the WIEN2K package [39]. Appendix B shows that the inclusion of the spin-orbit interaction within the second-variational method does not change the electronic structure close to the Fermi energy for the compounds with the heavy elements bismuth and moscovium because of the *s* symmetry of the states of interest. We employ the generalized gradient approximation (GGA) [40] for the exchange-correlation potential. For all our *s*-*p* systems, a simplified cubic $Pm\bar{3}m$ crystal structure is assumed, with both the tilting and breathing distortions neglected, and the volume is fully relaxed within GGA. The basis set size is fixed by setting $R_{\rm MT}K_{\rm max} = 7$, where $R_{\rm MT}$ is the smallest muffin-tin sphere radius and $K_{\rm max}$ is the cutoff wave vector. A $12 \times 12 \times 12$ grid of $\boldsymbol{k}$ points is used for integrating over the first Brillouin zone. Atomic and molecular orbital projections are done within muffin-tin spheres. Projections onto molecular orbitals are done with a modified version of WIEN2K, as discussed in Ref. [41]. Tight-binding (TB) parameters are obtained by using the maximally localized Wannier functions (MLWF) method as implemented in the WANNIER90 code [42].

III. RESULTS AND DISCUSSION

Let us first discuss the systematic series of ABO_3 *s*-*p* cubic perovskites, where the *A* and *B* cations are varied down the periodic table as $MgPO_3$, $CaAsO_3$, $SrSbO_3$, $BaSbO_3$, $SrBiO_3$, $BaBiO_3$, and $RaMcO_3$. Among them, only $SrBiO_3$, $BaSbO_3$, and $BaBiO_3$ exist in nature (see Table I), but our prime interest is to identify general trends in the electronic structure of such *s*-*p* systems.

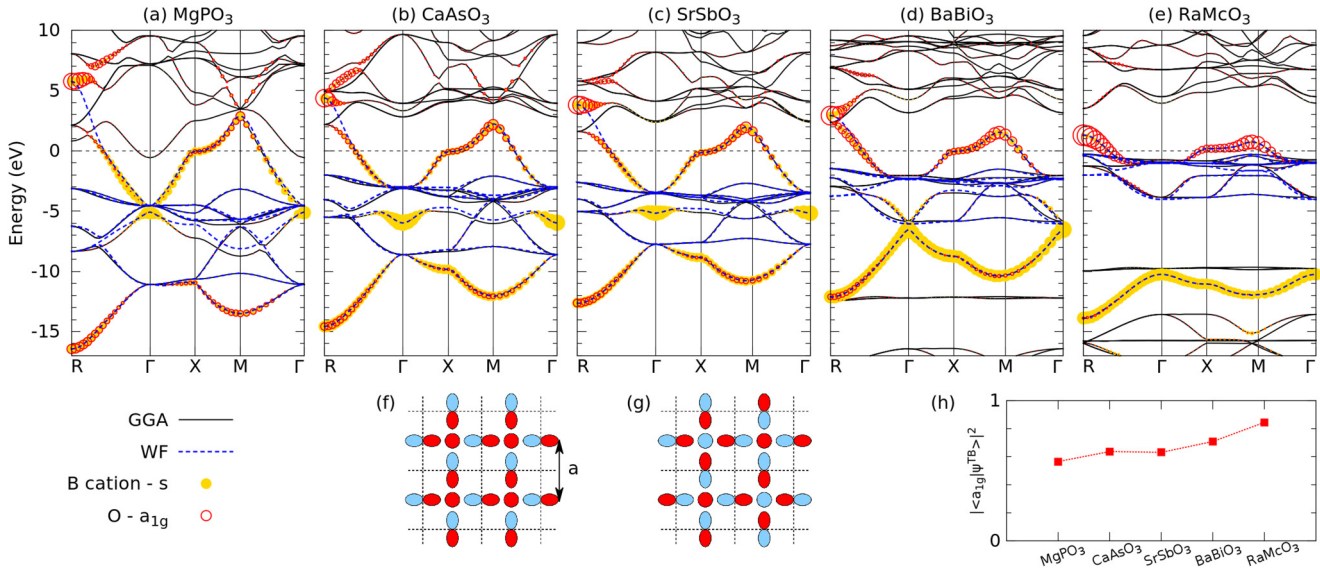

FIG. 2. The electronic band structures of (a) $MgPO_3$, (b) $CaAsO_3$, (c) $SrSbO_3$, (d) $BaBiO_3$, and (e) $RaMcO_3$ calculated in GGA and plotted with black solid lines. The Fermi energy is set to zero and marked by a horizontal black dashed line. The red and yellow circles indicate, respectively, the presence of the O a_{1g} and cation B s orbital characters in a given Bloch eigenstate, with the amount of their contribution being proportional to the circles' radii. The dashed blue lines represent the eigenstates of the MLWF-based TB model. (f) and (g) use a two-dimensional (2D) analog of the cubic perovskite structure to explain the absence of hybridization between the O $2p_\sigma$ and B s Bloch functions at the Γ point [$\boldsymbol{k} = (0, 0, 0)$] and its maximum strength at the R point [$\boldsymbol{k} = (\pi, \pi, \pi)$], respectively. The dashed lines mark boundaries between 2D unit cells with the lattice constant a. (h) The amount of the O a_{1g} molecular orbital character in the antibonding band of the ABO_3 TB models, $|\langle a_{1g}(\boldsymbol{k})|\psi^{\mathrm{TB}}(\boldsymbol{k})\rangle|^2$, at the R point as a function of chemical composition.

Figures 2(a)–2(e) and 3(a)–3(e) show the band structures and the projected densities of states (DOSs) of the studied ABO_3 series, respectively. Note that no results for $SrBiO_3$ and $BaSbO_3$ are shown as they are very similar to those for $BaBiO_3$ and $SrSbO_3$, respectively. All the systems demonstrate the same strong bonding-antibonding splitting between the B s atomic and O a_{1g} molecular orbitals, with the antibonding band landing at the Fermi level and becoming half occupied. Only in $MgPO_3$ is there a second band crossing the Fermi level, which is mainly of the Mg $3s$ orbital character. As a general trend, the overall bandwidth of the B s-O $2p$ states decreases as we go down from $MgPO_3$ to $RaMcO_3$. Indeed, as the lattice constant increases due to the large ionic radii of the A and B cations (see Table I), the direct hopping between oxygen orbitals decreases, which results in the reduction of the oxygen orbitals' bandwidth, and the hopping between oxygen orbitals and the B cation s orbitals also decreases, which results in the reduction of the bandwidth of the B s and O a_{1g} hybrid. On one hand, the narrowing of the oxygen band makes it easier to push the a_{1g} states up and out of the top of the oxygen band. On the other hand, the reduced B s-O $2p_\sigma$ hopping integral $t_{sp\sigma}$ leads to a flattening of the antibonding conduction band in $BaBiO_3$ and, especially, $RaMcO_3$. Correspondingly, the density of states at the Fermi level is strongly increased in these two end-members of the series, which makes them more strongly driven towards bond disproportionation and other types of structural distortions. Another important trend in the band structures of the ABO_3 series is the gradual change in the dominating character of the antibonding conduction band from one of more B s atomic orbital character to one of more O a_{1g} MO character. This is illustrated in Fig. 2(h), which shows the amount of the O a_{1g} MO character in the antibonding band of the ABO_3 TB models (which will be discussed in more detail shortly), $|\langle a_{1g}(\boldsymbol{k})|\psi^{\mathrm{TB}}(\boldsymbol{k})\rangle|^2$, at the R point as a function of chemical composition.

It is important to note that the bonding-antibonding splitting is strongly $\boldsymbol{k}$ vector dependent due to the changing symmetry of the Bloch functions involved. The splitting vanishes at Γ [$\boldsymbol{k} = (0, 0, 0)$] because at this point the Bloch wave function has no a_{1g} molecular orbital component [Fig. 2(f)]. In contrast, at the R point [$\boldsymbol{k} = (\pi, \pi, \pi)$], the Bloch wave function is of a pure a_{1g} molecular orbital character in the oxygen p_σ orbitals' domain [Fig. 2(g)], and the splitting reaches its maximum.

In accordance with this logic, the band structure plots in Fig. 2 feature no a_{1g} character in any of the Bloch states at the Γ point. Also, there is only one state with a dominating B s character at this $\boldsymbol{k}$ vector, which moves to lower energies towards the end of the ABO_3 series, from around -5 eV in $MgPO_3$ to -10 eV in $RaMcO_3$. Along the Γ-R path (and, actually, at any point other than Γ), the finite B s-O $2p_\sigma$ hybridization is expected to make the bonding band disperse downwards and reach a minimum at R. While this is what we indeed observe in the band structures of $BaBiO_3$ and $RaMcO_3$, the behavior of the bonding band in the band structures of $MgPO_3$, $CaAsO_3$, and $SrSbO_3$ appears to be more complex. There, the B s state at Γ happens to be energetically above the triply degenerate oxygen molecular orbital t_{1u} states (positioned at around -11 eV in $MgPO_3$ and -8 eV in $CaAsO_3$ and $SrSbO_3$). Away from Γ, these oxygen bands disperse upwards and get entangled with the bonding band. This is the reason why in $MgPO_3$, $CaAsO_3$, and $SrSbO_3$ the character of the bonding a_{1g} and B s combination is not continuous.

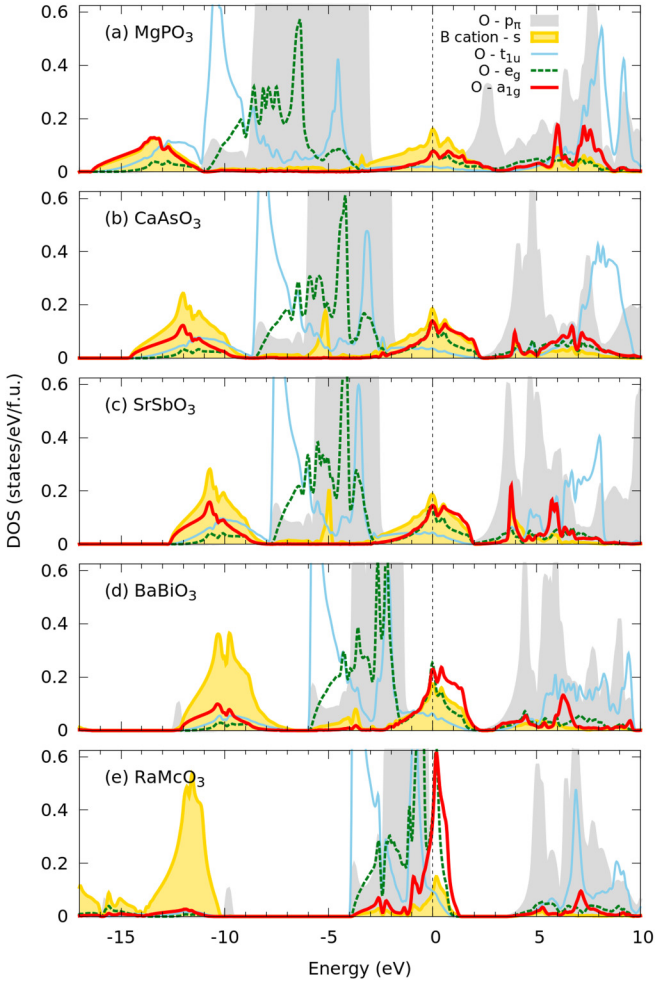

FIG. 3. The partial densities of states projected onto the B s atomic orbital and the molecular combinations of O $2p_\sigma$ orbitals of (a) $MgPO_3$, (b) $CaAsO_3$, (c) $SrSbO_3$, (d) $BaBiO_3$, and (e) $RaMcO_3$. The Fermi energy is set to zero and marked by a vertical black dashed line.

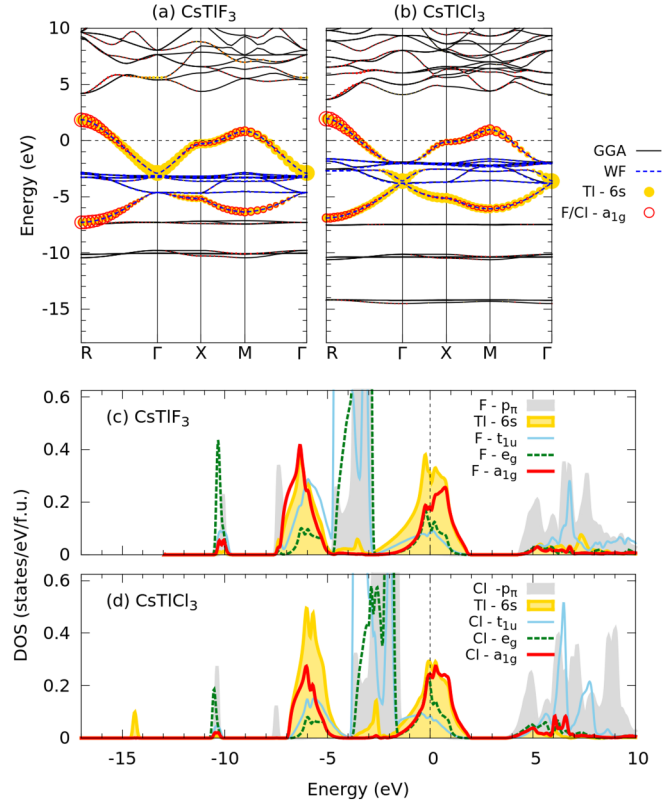

FIG. 4. The electronic band structures of (a) $CsTlF_3$ and (b) $CsTlCl_3$. Notations are similar to those in Fig. 2. Partial densities of states of (c) $CsTlF_3$ and (d) $CsTlCl_3$, projected onto the Tl $6s$ atomic orbital and the molecular combinations of the F $2p_\sigma$ or Cl $3p_\sigma$ orbitals. The zero of the energy is at the Fermi energy.

A similar situation occurs for the antibonding band close to the R point. At this point, in the same three systems, the interatomic orbital hybridizations are strong enough to push the antibonding state above the triply degenerate B p states and position it at around 4 to 6 eV. Away from R, the B p bands and the antibonding band mix with each other, and this is the reason why in these three systems the character of the antibonding a_{1g} and B s combination is not continuous either.

Let us now compare our findings about the ABO_3 series with the calculated electronic structures of $CsTlF_3$ and $CsTlCl_3$, shown in Fig. 4. These recently synthesized halides [34] also demonstrate the bond disproportionation, and so qualitatively, we expect their electronic structure near E_F to be very similar to the oxides, with O replaced by halogen and the divalent cation replaced with monovalent Cs, also resulting in divalent Tl formally with one electron in a $6s$ orbital, similar to the tetravalent Bi-based problem. It remains unknown, however, whether hole doping can make the thallium halides superconduct [43]. While we note an overall similarity to the electronic structure of the previously discussed ABO_3 compounds, the Tl $6s$-halogen a_{1g} band splitting is considerably smaller. Also, even though the difference between the $CsTlF_3$ and $CsTlCl_3$ lattice constants is quite significant (Table I), we see only a slight change in the bandwidths of their Tl $6s$-halogen a_{1g} band manifolds.

We proceed now to quantifying the observed differences in the electronic structures of the ABX_3 compounds in terms of the B s-X p hybridization strength $t_{sp\sigma}$ and the charge-transfer energy Δ. As shown in Ref. [26], these are the two main parameters that determine the character of the empty states right above the Fermi level. We should emphasize that in our convention Δ is defined using the electron language as the difference between the on-site energies of the B s atomic orbital and of the X a_{1g} MO: $\Delta = \epsilon(B\,s) - \epsilon(X\,a_{1g})$ [26]. $t_{sp\sigma}$ and Δ are obtained by calculating MLWF-based TB models for our systems. Similar to Ref. [24], here we consider 10 orbitals per formula unit: one B s and three X p orbitals per each of the three anions in a simple cubic unit cell. As one can see in Figs. 2(a)–2(e) and 4(a)–4(b), the resulting TB models have band dispersions that agree well with the GGA band structures. However, a small deviation exists at the R point in $MgPO_3$, $CaAsO_3$, and $SrSbO_3$ due to hybridization with higher-energy states, as discussed earlier. We have chosen not to consider the higher-energy B p orbitals in the TB models because our main focus is on the low-energy-scale electron

removal and addition states relevant for the physical properties at relatively low temperatures.

The hopping integrals $t_{sp\sigma}$ are given in Table I, while the atomic orbital energies with the complete set of Slater-Koster parameters are given in Appendix A. While for the ABO_3 series the value of $t_{sp\sigma}$ decreases rather monotonically from $MgPO_3$ to $RaMcO_3$ and is inversely related to the unit cell size, the $t_{sp\sigma}$ values of the two halides are surprisingly similar given the big difference between their unit cell sizes. In order to obtain the charge-transfer energy $\Delta = \epsilon(B\ s) - \epsilon(X\ a_{1g})$, we have applied a basis set transformation from oxygen atomic to oxygen molecular orbitals using the table in Fig. 1(b). This is a unitary transformation for the six O p_σ orbitals in the 2 f.u. supercell that is commensurate with the breathing distortion. The resulting charge-transfer energy values Δ are listed in Table I. In the ABO_3 series, Δ varies widely from a positive value of 1.83 eV in $MgPO_3$ to a negative value of -8.86 eV in $RaMcO_3$, thus marking a difference between $MgPO_3$ and $CsTlF_3$ as being *positive charge-transfer energy* compounds and the rest of the ABO_3 systems and $CsTlCl_3$ as being *negative charge-transfer energy* compounds. We note again that in all cases, except perhaps $RaMcO_3$, the total bonding-antibonding splitting strongly dominates over the charge-transfer energy, making the latter less important than the hopping integrals.

The dramatic decrease of Δ in the ABO_3 series with A and B moving down the periodic table can be understood in terms of relativistic lowering of the 6*s* and 7*s* orbital energies in the heavy elements Bi and Mc [44]. In $RaMcO_3$, it takes an extreme form, which, combined with the reduced $t_{sp\sigma}$ hybridization, results in an almost ionic character of the Mc^{3+} ionization state, in agreement with earlier studies [45]. This can be clearly seen from the $RaMcO_3$ projected DOS shown in Fig. 3(e). Similar to $Ba(Sr)BiO_3$, $RaMcO_3$ is therefore expected to bond disproportionate in its ground state as $2Mc^{3+}\underline{L}^2 \rightarrow [Mc^{3+}]_{\text{large}} + [Mc^{3+}\underline{L}^2]_{\text{small}}$, with most of the action happening on oxygens. We should also note that the density of states at E_F is very high in $RaMcO_3$ because of the narrowing of the antibonding band, and this could support a higher T_c. Of course, as far as this superheavy-element compound is concerned, with only around 100 Mc atoms having been made so far (which are also radioactive, with a half-life of 0.65 seconds), experimental realization/investigation of $RaMcO_3$ will most likely not be possible in the foreseeable future. Fortunately, superconducting K- and Pb-doped antimonates are experimentally available [36,37]. Rather interesting is the fact that $BaSbO_3$ can become superconducting upon substituting Sb with Pb but not with Sn [36]. This was explained in terms of the relativistic energy lowering of Pb 6*s* states with respect to Sn 5*s* states [35]. However, the maximal T_c observed in $BaPb_xSb_{1-x}O_3$ is 3.5 K, which is considerably lower than that of the bismuthates. On the other hand, the most recently discovered superconducting K-doped barium antimonates [37], with T_c reaching a maximum of 15 K at the doping concentration $x = 0.65$, follow the opposite trend since in the K-doped bismuthates T_c is more than a factor of 2 smaller at the same doping concentration. Given these conflicting behaviors of the A and B cation substituted antimonates, we can only speculate about the relation between T_c and how negative Δ is. If a strongly negative Δ is crucial for a robust superconducting state, then optimally hole doped $RaMcO_3$ might have a very high T_c. Conversely, if the highest level of hybridization between the B *s* and X a_{1g} orbitals is important, which is achieved by, primarily, $t_{sp\sigma}$ being large but also by Δ having a small absolute value, then the superconducting coupling should increase as one moves up the periodic table. In order to identify the realistic scenario and understand the underlying physics, more theoretical and experimental studies on *s*-*p* perovskites are required.

Finally, with the hopping integrals $t_{sp\sigma}$ and charge-transfer energies Δ of our studied ABX_3 compounds at hand, we can mark their positions on the phase diagram proposed in Ref. [26]. There will be some degree of approximation involved because this phase diagram was obtained for $BaBiO_3$ in a bond-disproportionated state using the value of the oxygen bandwidth W specific to $BaBiO_3$, but this will not obscure observation of the general trends that we are most interested in. As explained in Ref. [26], the colors in this phase diagram represent the dominant character of the empty (hole) states above the Fermi level as a function of hybridization and charge-transfer energy. While there is a sharp boundary around the green region where holes reside on X e_g orbitals, the B *s* (yellow) and X a_{1g} (red) orbitals are always mixed by hybridization, and therefore, there is a gradual crossover between the yellow and red regions. As we argued in Ref. [26], if the holes in a given *s*-*p* system are of the B *s* character, the breathing distortion that the system might undergo corresponds to charge disproportionation between the B cations. Conversely, if the holes are of the X a_{1g} character, the breathing distortion would, rather, correspond to bond disproportionation, with little actual charge transfer happening. Even though we presently consider simple cubic cells without the breathing distortion, this correspondence between the holes' character and the type of disproportionation is emphasized in the phase diagram in Fig. 5 by labeling the red region as "X a_{1g} (BD)" and the yellow region as "B *s* (CD)." The black dashed line marks equal contributions from the B *s* and X a_{1g} orbitals to the holes' character. Figure 5 shows now that $SrBiO_3$ and $BaBiO_3$ are relatively deep in the X a_{1g} region, while $MgPO_3$, $CaAsO_3$, $SrSbO_3$, $BaSbO_3$, and $CsTlF_3$ are close to having equal B *s* and X a_{1g} orbital contributions. As for $RaMcO_3$ and $CsTlCl_3$, they land in the O e_g region, but from their projected DOSs [Figs. 3(e) and 4(d)] we know that their hole character is strongly O a_{1g}. This discrepancy is due to the mentioned approximations, but it is obvious that $RaMcO_3$ must, in any case, be located very far inside the O a_{1g} region close to the O e_g border.

IV. CONCLUSIONS

In this paper, we have used *ab initio* methods to study the electronic structures of the following ABX_3 *s*-*p* cubic perovskites: the experimentally available $BaSbO_3$, $SrBiO_3$, $BaBiO_3$, $CsTlF_3$, and $CsTlCl_3$, as well as the hypothetical $MgPO_3$, $CaAsO_3$, $SrSbO_3$, and $RaMcO_3$. We have used Wannier function based tight-binding modeling to calculate the hybridization strengths $t_{sp\sigma}$ between the B *s* and X *p* atomic orbitals and charge-transfer energies Δ, which are the two most important parameters that determine the nature of the systems' holes. These calculations have elucidated several

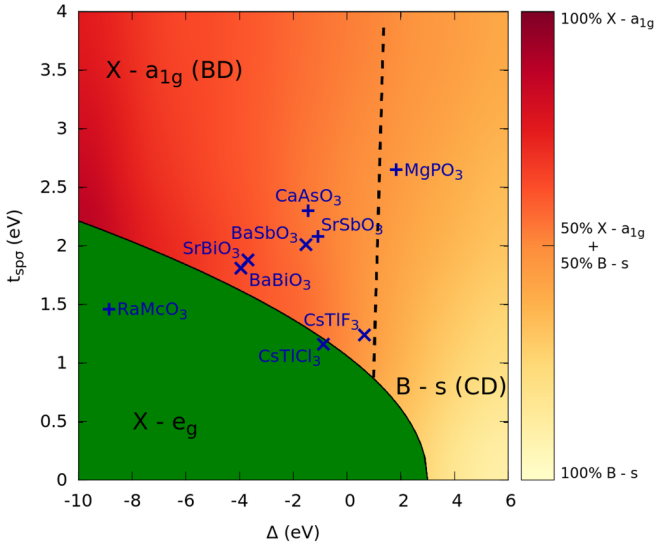

FIG. 5. The phase diagram of Ref. [26] representing the dominant character of holes as a function of the charge-transfer energy Δ and hybridization $t_{sp\sigma}$. The + and × symbols mark the parameters relevant to the hypothetical and existing cubic *s-p* ABX_3 perovskites, respectively. Green, yellow, and red colors represent the amount of X e_g, X a_{1g}, and B cation s orbital contributions to the holes' character, respectively.

trends in $t_{sp\sigma}$ and Δ as one moves across the periodic table, such as the relativistic energy lowering of the B s orbital in heavy B cations leading to strongly negative Δ values. Our results have been discussed in connection with the general phase diagram for *s-p* cubic perovskites proposed in Ref. [26].

Also, some considerations were offered regarding a possible relation between the highest achievable superconducting transition temperatures and certain features of the systems' electronic structures, such as the charge-transfer energy Δ and the interatomic orbital hybridization B s-O $2p_\sigma$ $t_{sp\sigma}$, with the latter primarily controlling the conduction bandwidth and the DOS at the Fermi level. In particular, we observed that the more negative the Δ value is, the greater the X a_{1g} character will be in the valence and conduction bands, provided that the hybridization strength is large enough to still push out the X a_{1g} bound state. In the case of $RaMcO_3$ and also $Ba(Sr)BiO_3$, Δ is very negative, and so the amount of the X a_{1g} character in the antibonding state will be the largest. As Δ becomes even more negative, there will be a point where the X a_{1g} state is no longer pushed above the X e_g state, as illustrated in the phase diagram in Fig. 5. While the relation between the electronic structure parameters Δ and $t_{sp\sigma}$ and the superconducting coupling strength still needs to be investigated in future theoretical and experimental studies, a very important feature of the electronic structure that could be responsible for an enhanced T_c is the increase of the DOS at the Fermi level in $BaBiO_3$ due to its reduced $t_{sp\sigma}$ value. For these reasons, we expect that optimally hole doped $RaMcO_3$ might have an increased T_c as well.

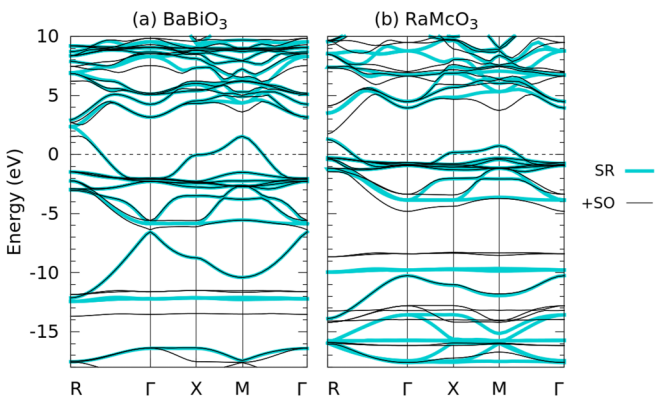

FIG. 6. The electronic band structures of (a) $BaBiO_3$ and (b) $RaMcO_3$ calculated within the scalar-relativistic approximation (SR) and using a second-variational method to account for spin-orbit interaction (+SO). The zero of the energy is at the Fermi energy.

ACKNOWLEDGMENTS

This research was undertaken thanks, in part, to funding from the Max Planck-UBC-UTokyo Center for Quantum Materials and the Canada First Research Excellence Fund, Quantum Materials and Future Technologies Program as well as from CIFAR.

APPENDIX A

This Appendix provides atomic orbital energies and Slater-Koster parameters for the studied ABX_3 compounds, which are given in Table II and are related to the TB parameters in Table I through a unitary transformation. One should consider, however, that the 10 orbital TB models derived and analyzed in this paper also feature rather large next-nearest-neighbor interatomic hopping integrals that compensate the absence of the B cation p orbitals from the basis. Therefore, using only the nearest-neighbor hopping integrals from Table II will result in a poor match between the model band structures and the DFT ones.

APPENDIX B

Since bismuth, with an atomic number of 83, and, especially, moscovium, with an atomic number of 115, are heavy

TABLE II. GGA-based atomic orbital energies and Slater-Koster parameters of the studied ABX_3 cubic perovskites (in eV).

	ε_s	ε_{p_σ}	ε_{p_π}	$(sp\sigma)$	$(pp\sigma)$	$(pp\pi)$
$MgPO_3$	-5.44	-8.11	-5.61	2.65	1.13	-0.16
$CaAsO_3$	-6.51	-5.95	-3.80	2.30	0.74	-0.16
$SrSbO_3$	-5.67	-5.52	-4.08	2.08	0.56	-0.10
$BaSbO_3$	-5.70	-5.15	-3.59	2.01	0.43	-0.08
$SrBiO_3$	-6.97	-4.12	-2.96	1.88	0.45	-0.10
$BaBiO_3$	-6.99	-3.86	-2.75	1.81	0.46	-0.10
$RaMcO_3$	-10.53	-2.16	-1.31	1.46	0.34	-0.09
$CsTlF_3$	-2.69	-3.73	-3.30	1.24	0.09	-0.02
$CsTlCl_3$	-3.36	-2.75	-2.23	1.16	0.23	-0.04

elements, relativistic effects beyond the scalar-relativistic approximation may be important in the cases of $BaBiO_3$ and $RaMcO_3$. In order to investigate whether these effects could affect the conclusions of our present study, we performed additional calculations for these two compounds with the spin-orbit interaction included within the second-variational approach based on scalar-relativistic orbitals [39]. Their electronic band structures calculated with and without the spin-orbit interaction are compared in Fig. 6. Even in $RaMcO_3$, where the relativistic effects are the strongest, although the bands with a finite Mc $7p$ orbital contribution (e.g., at around 4 eV at the R point) are indeed visibly affected by the spin-orbit interaction, the Mc $7s$ and O a_{1g} bonding and antibonding bands are barely changed. This observation is in accordance with the Mc $7s$ electrons having no orbital angular momenta and thus not being affected by the spin-orbit interaction. Since considering the spin-orbit interaction does not change the character and the dispersion of the antibonding band crossing the Fermi level in $BaBiO_3$ and $RaMcO_3$ even quantitatively, our derived low-energy Hamiltonians for these two systems and our conclusions regarding their superconducting properties remain valid.

[1] M. Imada, A. Fujimori, and Y. Tokura, Rev. Mod. Phys. **70**, 1039 (1998).
[2] M. L. Medarde, J. Phys.: Condens. Matter **129**, 1679 (1997).
[3] J. G. Bednorz and K. A. Muller, Z. Phys. B **64**, 189 (1986).
[4] A. W. Sleight, J. L. Gillson, and P. E. Bierstedt, Solid State Commun. **17**, 27 (1975).
[5] R. J. Cava, B. Batlogg, J. J. Krajewski, R. Farrow, L. W. Rupp, Jr., A. E. White, K. Short, W. F. Peck, and T. Kometani, Nature (London) **332**, 814 (1988).
[6] A. M. Green, A. Ho-Baillie, and H. J. Snaith, Nat. Photonics **8**, 506 (2014).
[7] A. P. Ramirez, J. Phys.: Condens. Matter **9**, 8171 (1997).
[8] T. Kimura, T. Goto, H. Shintani, K. Ishizaka, T. Arima, and Y. Tokura, Nature (London) **426**, 58 (2003).
[9] H. Jin, S. H. Rhim, J. Im, and A. J. Freeman, Sci. Rep. **3**, 1651 (2013).
[10] H. Jin, J. Im, and A. J. Freeman, Phys. Rev. B **86**, 121102(R) (2012).
[11] B. Yan, M. Jansen, and C. Felser, Nat. Phys. **9**, 709 (2013).
[12] L. F. Mattheiss, E. M. Gyorgy, and D. W. Johnson, Jr., Phys. Rev. B **37**, 3745(R) (1988).
[13] S. M. Kazakov, C. Chaillout, P. Bordet, J. J. Capponi, M. Nunez-Regueiro, A. Rysak, J. L. Tholence, P. G. Radaelli, S. N. Putilin, and E. V. Antipov, Nature (London) **390**, 148 (1997).
[14] D. Cox and A. W. Sleight, Solid State Commun. **19**, 969 (1976).
[15] D. E. Cox and A. W. Sleight, Acta Crystallogr., Sect. B **35**, 1 (1979).
[16] Q. Zhou and B. J. Kennedy, Solid State Commun. **132**, 389 (2004).
[17] A. Sleight, Phys. C (Amsterdam, Neth.) **514**, 152 (2015).
[18] C. M. Varma, Phys. Rev. Lett. **61**, 2713 (1988).
[19] A. Taraphder, H. R. Krishnamurthy, R. Pandit, and T. V. Ramakrishnan, Phys. Rev. B **52**, 1368 (1995).
[20] I. Hase and T. Yanagisawa, Phys. Rev. B **76**, 174103 (2007).
[21] L. F. Mattheiss and D. R. Hamann, Phys. Rev. B **28**, 4227 (1983).
[22] W. A. Harrison, Phys. Rev. B **74**, 245128 (2006).
[23] K. Foyevtsova, A. Khazraie, I. Elfimov, and G. A. Sawatzky, Phys. Rev. B **91**, 121114(R) (2015).
[24] A. Khazraie, K. Foyevtsova, I. Elfimov, and G. A. Sawatzky, Phys. Rev. B **97**, 075103 (2018).
[25] G. M. Dalpian, Q. Liu, J. Varignon, M. Bibes, and A. Zunger, Phys. Rev. B **98**, 075135 (2018).
[26] A. Khazraie, K. Foyevtsova, I. Elfimov, and G. A. Sawatzky, Phys. Rev. B **98**, 205104 (2018).
[27] J. de Hair and G. Blasse, Solid State Commun. **12**, 727 (1973).
[28] A. F. Orchard and G. Thornton, J. Chem. Soc. Dalton Trans. 1238 (1977).
[29] G. K. Wertheim, J. P. Remeika, and D. N. E. Buchanan, Phys. Rev. B **26**, 2120 (1982).
[30] S. Salem-Sugui, Jr., E. E. Alp, S. M. Mini, M. Ramanathan, J. C. Campuzano, G. Jennings, M. Faiz, S. Pei, B. Dabrowski, Y. Zheng, D. R. Richards, and D. G. Hinks, Phys. Rev. B **43**, 5511 (1991).
[31] N. C. Plumb, D. J. Gawryluk, Y. Wang, Z. Ristic, J. Park, B. Q. Lv, Z. Wang, C. E. Matt, N. Xu, T. Shang, K. Conder, J. Mesot, S. Johnston, M. Shi, and M. Radovic, Phys. Rev. Lett. **117**, 037002 (2016).
[32] S. Balandeh, R. J. Green, K. Foyevtsova, S. Chi, O. Foyevtsov, F. Li, and G. A. Sawatzky, Phys. Rev. B **96**, 165127 (2017).
[33] H. Raebiger, S. Lany, and A. Zunger, Charge self-regulation upon changing the oxidation state of transition metals in insulators, Nature (London) **453**, 763 (2008).
[34] M. Retuerto, T. Emge, J. Hadermann, P. W. Stephens, M. R. Li, Z. P. Yin, M. Croft, A. Ignatov, S. J. Zhang, Z. Yuan, C. Jin, J. W. Simonson, M. C. Aronson, A. Pan, D. N. Basov, G. Kotliar, and M. Greenblatt, Chem. Mater. **25**, 4079 (2013).
[35] D. J. Singh, D. A. Papaconstantopoulos, J. P. Julien, and F. Cyrot-Lackmann, Phys. Rev. B **44**, 9519 (1991).
[36] R. J. Cava, B. Batlogg, G. P. Espinosa, A. P. Ramirez, J. J. Krajewski, W. F. Peck, Jr., L. W. Rupp, Jr., and A. S. Cooper, Nature (London) **339**, 291 (1989).
[37] M. Kim, G. M. McNally, H.-H. Kim, M. Oudah, A. Gibbs, P. Manuel, R. Green, T. Takayama, A. Yaresko, U. Wedig, M. Isobe, R. K. Kremer, D. A. Bonn, B. Keimer, and H. Takagi, arXiv:2107.06596.
[38] W. Kohn and L. J. Sham, Phys. Rev. **140**, A1133 (1965).
[39] P. Blaha, K. Schwarz, G. K. H. Madsen, D. Kvasnicka, J. Luitz, R. Laskowski, F. Tran and L. D. Marks, *WIEN2k, An Augmented Plane Wave + Local Orbitals Program for Calculating Crystal Properties* (Karlheinz Schwarz, Techn. Universität Wien, Austria, 2018).

[40] J. P. Perdew, K. Burke, and M. Ernzerhof, Phys. Rev. Lett. **77**, 3865 (1996).
[41] K. Foyevtsova and G. A. Sawatzky, J. Mod. Phys. **10**, 953 (2019).
[42] A. A. Mostofi, J. R. Yates, Y.-S. Lee, I. Souza, D. Vanderbilt, and N. Marzari, Comput. Phys. Commun. **178**, 685 (2008).
[43] M. Retuerto, Z. Yin, T. J. Emge, P. W. Stephens, M.-R. Li, T. Sarkar, M. C. Croft, A. Ignatov, Z. Yuan, S. J. Zhang, C. Jin, R. P. Sena, J. Hadermann, G. Kotliar, and M. Greenblatt, Inorg. Chem. **54**, 1066 (2015).
[44] P. Pyykko, Chem. Rev. **88**, 563 (1988).
[45] O. L. Keller, Jr., C. W. Nestor, Jr., and B. Fricke, J. Phys. Chem. **78**, 1949 (1974).